J. Fluid Mech. (1977), *vol.* 83, *part* 3, *pp.* 415–431
Printed in Great Britain

Effects of horizontally two-dimensional bodies on the mass transport near the sea bottom

By JACQUES LAMOURE
Laboratoire Régional CETE de Bordeaux, France
AND CHIANG C. MEI
Department of Civil Engineering, Massachusetts Institute of Technology, Cambridge

(Received 5 January 1977 and in revised form 26 March 1977)

Mass transport close to the sea bottom is investigated for simple harmonic waves around a body with a small horizontal dimension. For gravity waves it is shown that the mass transport very near the bottom points towards a convex corner, but near the top of the boundary layer its direction reverses. Possible implications for silting near a pile and a harbour entrance are discussed and some experimental evidence given. For tides, the Coriolis force introduces a spiralling variation within the boundary layer, and possible inferences for coastline modification are drawn.

1. Introduction

The phenomenon of acoustic streaming near a wall was first shown by Rayleigh (1883) to be caused by viscosity in the boundary layer. Longuet-Higgins (1953) extended the theory to water waves and further showed that the Stokes drift must be superimposed on the preceding Eulerian drift in order to follow a dye particle. The sum, which is a Lagrangian quantity, is now called the *mass transport* velocity, knowledge of which is of interest in understanding the movement of sediments on the sea bottom. The details of two-dimensional problems (in x and z, horizontal and vertical) have been completed by Longuet-Higgins for arbitrary inviscid oscillatory flows outside the boundary layer. For three-dimensional gravity waves, general formulae for the Eulerian streaming have been worked out by Hunt & Johns (1963), who, however, gave only the mass transport near the outer edge of the viscous layer. In Kundt's tube with standing acoustic waves, it is known that the heavy dust particles tend to roll along the bottom towards the nodes, while the light particles tend to drift in suspension towards the antinodes. Similar behaviour is also observed in gravity waves. This is clearly the effect of the vertical variation of mass transport through the boundary layer. For arbitrary inviscid oscillatory flows, such variation can be inferred from the Eulerian results of Hunt & Johns as by Carter, Liu & Mei (1973), who also demonstrated in a wave tank the influence of mass transport near the solid bottom on the tendency to sand-bar formation. Relevant field evidence of submarine bars near Escambia Bay, Florida, has been pointed out by Lau & Travis (1973). The formulae of Carter *et al.* are given in terms of derivatives of the inviscid oscillatory velocity field just outside the boundary layer, so that it is in principle a straightforward matter to obtain the mass transport distribution for any complex

wave system. Thus far, however, applications have been limited to essentially one-dimensional waves or to simple obliquely incident and reflected waves, and physical consequences in truly two-dimensional waves (three-dimensional flows) have not been sufficiently explored.

In the case of tides in a rotating ocean, Hunt & Johns (1963) obtained, by assuming the tidal flow to be purely harmonic, results for the outer edge, but omitted the interior, of the bottom boundary layer. Specific applications are also for essentially one-dimensional waves. Moore (1970) further points out that the Eulerian drift outside the boundary layers of a rotating ocean is non-zero in general and is forced by non-linearity. The only strictly two-dimensional wave problem treated seems to be that studied by Longuet-Higgins (1970) for a small circular island, but is on the mass transport just outside the boundary layer near the vertical wall.

In this paper we discuss the effect of two-dimensional bodies, such as piles, breakwaters in gravity waves or islands and estuaries in tides, whose characteristic dimensions are much less than the wavelength. In gravity waves an explicit formula is inferred from Carter *et al.* which leads to interesting physical consequences for bodies of engineering interest. Experimental evidence of the induced sediment motion is given. In tides, new results for the mass transport throughout the bottom boundary layer are derived on the basis of constant viscosity. Ekman effects are brought out. Numerical results for a peninsula and an estuary are given.

2. Mass transport by gravity waves near a small body

2.1. *A general formula*

Let x and y be the local horizontal and z be the local vertical co-ordinates fixed on the sea bottom. Considering only monochromatic waves with frequency ω, the inviscid velocity field of the wave near the solid bottom may be denoted by

$$\mathbf{U}_I = \mathrm{Re}\,(U_0 e^{i\omega t}, V_0 e^{i\omega t}),$$

where $U_0 = U_0(x, y)$ and $V_0 = V_0(x, y)$. Using the model of constant viscosity, the horizontal components of the Lagrangian mass transport velocity within the Stokes boundary layer $0 < z/\delta < \infty$, $\delta = (2\nu/\omega)^{\frac{1}{2}}$, are given by Carter *et al.* as follows:

$$\langle u_L \rangle = \frac{1}{4\omega}\mathrm{Re}\left[G_1 U_0 \frac{\partial U_0^*}{\partial x} + G_2 V_0 \frac{\partial U_0^*}{\partial y} + (G_1 - G_2) U_0 \frac{\partial V_0^*}{\partial y}\right], \tag{2.1}$$

$$\langle v_L \rangle = \frac{1}{4\omega}\mathrm{Re}\left[G_1 V_0 \frac{\partial V_0^*}{\partial y} + G_2 U_0 \frac{\partial V_0^*}{\partial x} + (G_1 - G_2) V_0 \frac{\partial U_0^*}{\partial x}\right], \tag{2.2}$$

where

$$\left.\begin{aligned} G_1 &= 8ie^{-(1+i)\xi} + 3(1-i)e^{-2\xi} - 3 - 5i, \\ G_2 &= 4ie^{-(1+i)\xi} + (1-2i)e^{-2\xi} - 1 - 2i, \end{aligned}\right\} \quad \xi \equiv z/\delta. \tag{2.3}$$

The above result does not hold in a small corner within a horizontal distance $O(\delta)$ from the vertical wall.

We remark that the oscillatory boundary layer near a sea bottom is usually turbulent. From experiments with turbulent boundary layers on rough bottoms, the order of magnitude of the eddy viscosity is $10 \sim 100\,\mathrm{cm^2/s}$, except near the wall. The corresponding estimates for δ are $5{\cdot}6 \sim 17{\cdot}8\,\mathrm{cm}$ for a typical swell period of 10 s. It

must be pointed out that the eddy viscosity is known experimentally to be a function of z and t; see Johnson & Carlsen (1976) and Horikawa & Watanabe (1968). Since a complete picture is still lacking, the simplest model is adopted here.

Let us assume that the sea depth h is constant and that all solid bodies have vertical walls spanning the entire depth of water. The first-order inviscid flow field can then be described by

$$(u_1, v_1, w_1) = \mathrm{Re}\left(\frac{\partial\phi}{\partial x}, \frac{\partial\phi}{\partial y}, \frac{\partial\phi}{\partial z}\right) e^{i\omega t}, \tag{2.4}$$

where

$$\phi = \frac{ig\eta}{\omega} \frac{\cosh k(z+h)}{\cosh kh} e^{i\omega t}, \quad \omega^2 = gk \tanh kh \tag{2.5}$$

with η satisfying

$$\nabla^2\eta + k^2\eta = 0 \quad \text{outside the body} \quad (\nabla^2 = \partial^2/\partial x^2 + \partial^2/\partial y^2), \tag{2.6}$$

and

$$\partial\eta/\partial n = 0 \quad \text{on the body.} \tag{2.7}$$

If the controlling horizontal scale of the bodies a is so small that $ka \ll 1$, then it is well known that in the near field of the body, where $r/a = O(1)$, the Helmholtz equation may be approximated by the Laplace equation, which implies that locally the velocity field is incompressible and irrotational in the horizontal plane:

$$w_1 = O(kau_1), \quad \frac{\partial u_1}{\partial x} + \frac{\partial v_1}{\partial y} = O(ka)^2, \quad \frac{\partial u_1}{\partial y} - \frac{\partial v_1}{\partial x} = O(ka)^2. \tag{2.8a–c}$$

The same approximation holds for U_0 and V_0, where

$$(U_0, V_0) = \frac{ig}{\omega} \frac{1}{\cosh kh} \nabla\eta. \tag{2.9}$$

To the leading approximation the near-field velocity may be found by standard methods for steady potential flow, but is indeterminate up to a constant factor which may be found by matching with the inner approximation of the far field, for $kr = O(1)$. Although this analysis may be carried out (see, for example, Buchwald 1971; Mei & Ünlüata 1976; etc.) it is unimportant for our purposes here and will not be pursued. Since U_0 and V_0 share the common factor of a complex constant, their phases drop out in (2.1) and (2.2). Hence U_0 and V_0 will be taken as real for brevity. Using (2.8) for U_0 and V_0 we easily obtain the simple result that

$$\langle \mathbf{u}_L \rangle = (2\omega)^{-1} H_L(\xi) \nabla |\mathbf{U}_0|^2, \tag{2.10}$$

where

$$H_L = \tfrac{1}{4} \mathrm{Re}\, G_2 = \tfrac{1}{4}(4e^{-\xi} \sin\xi + e^{-2\xi} - 1) \tag{2.11}$$

and $\mathbf{U}_0 \equiv (U_0, V_0)$. This is a simple result stating that at any height ξ the vector $\langle \mathbf{u}_L \rangle$ has either the same or the opposite direction to the gradient vector $\nabla|\mathbf{U}_0|^2$ of the inviscid field. Thus $\langle \mathbf{u}_L \rangle$ is maximum where $\nabla|\mathbf{U}_0|^2$ is maximum, which usually, but not necessarily, occurs at sharp convex corners. The vertical variation is given by the factor $H_L = \frac{1}{4}\mathrm{Re}\, G_2$, which changes sign at about $z \cong \delta$ as plotted in figure 1. In particular,

$$\langle \mathbf{u}_L \rangle \cong \xi(4\omega)^{-1} \nabla |\mathbf{U}_0|^2 \quad \text{for} \quad \xi \ll 1 \tag{2.12a}$$

and

$$\langle \mathbf{u}_L \rangle \cong -(8\omega)^{-1} \nabla |\mathbf{U}_0|^2 \quad \text{for} \quad \xi \gg 1. \tag{2.12b}$$

Thus, near a sharp corner, where the inviscid velocity has the largest gradient, the mass transport is greatest, and is directed towards the corner near the bottom of the boundary layer and away from the corner near the top of the boundary layer.

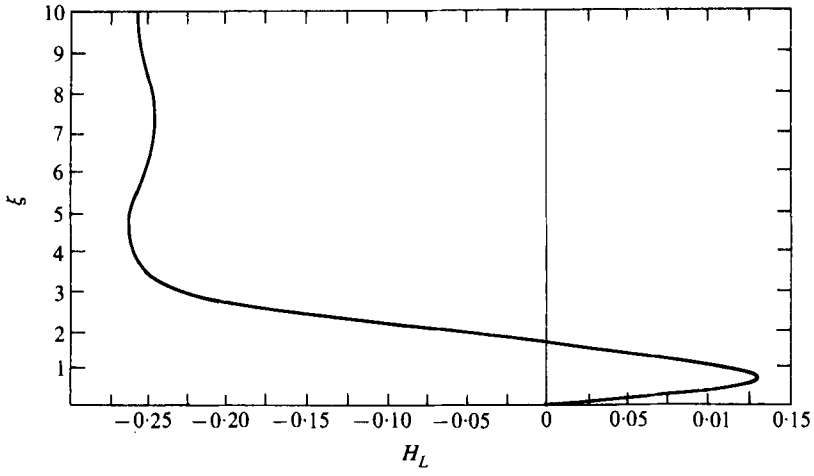

FIGURE 1. Vertical variation of Lagrangian mass transport in gravity waves near a small body; $\xi = z/\delta$.

It should be pointed out that in the near field the Stokes drift, defined by

$$\langle \mathbf{u}_S \rangle = \left\langle \left(\int \mathbf{u}_1 dt \right) . \nabla \mathbf{u}_1 \right\rangle + \left\langle \left(\int w_1 dt \right) \frac{\partial \mathbf{u}_1}{\partial z} \right\rangle, \tag{2.13}$$

is negligible for small ka, so that the mass transport is just the Eulerian drift. This is due partly to the fact that the second term on the right of (2.13) is negligible; see (2.8a). Furthermore, in non-rotating fluids $\mathbf{u}_1$ and $\mathbf{U}_I$ are coplanar and proportional to each other. Since $\mathbf{U}_0$ may be taken to be real, the two factors in the first term of (2.13) are out of phase by $\frac{1}{2}\pi$, which implies a zero average for their product.

With regard to sediment transport, the above results suggest that heavy sediment, once mobilized by the first-order velocity field to roll on the bottom, may be attracted towards and deposited near a convex corner. This striking result may appear puzzling as one would instinctively feel that sediment should accumulate near the stagnation points, where $U_0 = V_0 = 0$, and be swept away where (U_0, V_0) is large. The following explanation may help to clarify the physical mechanism.

Consider a vertical column of fluid of unit square cross-section with its base at the level z inside the boundary layer and its top at the outer edge of the boundary layer. The net mean stresses acting on the column are the mean shear stress at the base $\mu \partial \langle \mathbf{u} \rangle / \partial z$, the mean normal pressure gradient $\frac{1}{2}\rho \nabla \mathbf{U}_I^2$ and the gradient of the normal Reynolds stress $-\frac{1}{2}\rho \langle \nabla \mathbf{u}_1^2 \rangle$, the last two acting on the vertical sides. Because $w_1 \cong 0$, the shear components of the Reynolds stress are negligible. Equating the forces, we have

$$\mu \frac{\partial \langle \mathbf{u} \rangle}{\partial z} = \frac{1}{2}\rho \int_z^\infty \nabla \langle \mathbf{U}_I - \mathbf{u}^2 \rangle \, dz.$$

The integral on the right side is clearly coplanar with and proportional to $\nabla \mathbf{U}_0^2$; so, therefore, is $\langle \mathbf{u} \rangle$.

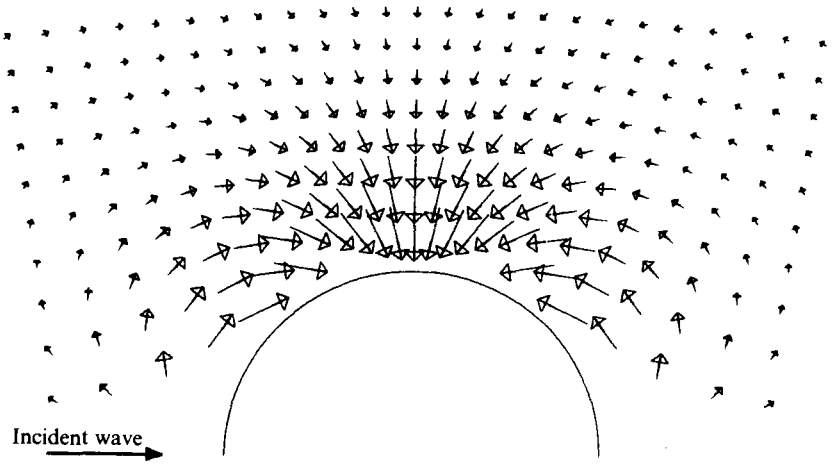

FIGURE 2. Mass transport velocity vectors in gravity waves near the solid bottom in the presence of a circular cylinder.

2.2. *Examples*

As a first example we take a circular pile rising vertically from the sea bottom to the free surface. If the incident wave is directed along the $-x$ axis the free-surface displacement in the near field ($ka = O(1)$) is approximately

$$\eta \cong A[1 + ik\cos\theta(r + a^2/r)], \tag{2.14}$$

where (r, θ) are polar co-ordinates with origin at the centre of the cylinder, whose radius is a. The corresponding components $\langle u_L\rangle_r$ and $\langle u_L\rangle_\theta$ of the mass transport can be calculated to be

$$\begin{bmatrix}\langle u_L\rangle_r \\ \langle u_L\rangle_\theta\end{bmatrix} = \left(\frac{gkA}{\omega\cosh kh}\right)^2 \frac{4}{a}\left(\frac{a}{r}\right)^3 \begin{bmatrix}-a^2/r^2 + \cos 2\theta \\ \sin 2\theta\end{bmatrix} \frac{1}{2\omega} H_L(\xi). \tag{2.15}$$

In figure 2, the mass transport vectors $\langle \mathbf{u}_L\rangle$ near the bottom ($\xi < 1{\cdot}6$) are plotted for the region $y > 0$. There is a convergence towards the points $r = a$, $\theta = \pm\frac{1}{2}\pi$, which are on the diameter parallel to the crests. Near the points on the diameter perpendicular to the crests ($r = a$, $\theta = 0, \pi$), $\langle \mathbf{u}_L\rangle = 0$. The directions of the vectors are reversed for $\xi > 1{\cdot}6$ while the magnitudes remain in the same proportion. Note that adding a right-going wave of a different amplitude simply changes the factor Aik in (2.14) to a different complex constant, but does not change the relative magnitude of $\langle \mathbf{u}_L\rangle$. The same is true if the cylinder is in a partially standing wave.

The case of an elliptical pile with principal axes a and b can be easily worked out using the Joukowski transformation; see Lamoure (1976).

As another example, let us consider a semi-infinite breakwater with a rectangular head of thickness $2a$. The diffraction problem for small ka has been studied by Crighton & Leppington (1973) by the method of matched asymptotics. The potential solution in the near field may be approximated by

$$\eta \cong (4A/\pi)e^{\frac{1}{4}i\pi}(ka)^{\frac{1}{2}}\cos\tfrac{1}{2}\theta_i \operatorname{Re}\tau(Z/a), \tag{2.16}$$

where τ is the following analytic function of the complex variable $Z = x + iy$:

$$\tfrac{1}{2}\pi(Z/a - i) = \tau(\tau^2 - 1)^{\frac{1}{2}} - \ln[\tau + (\tau^2 - 1)^{\frac{1}{2}}], \tag{2.17}$$

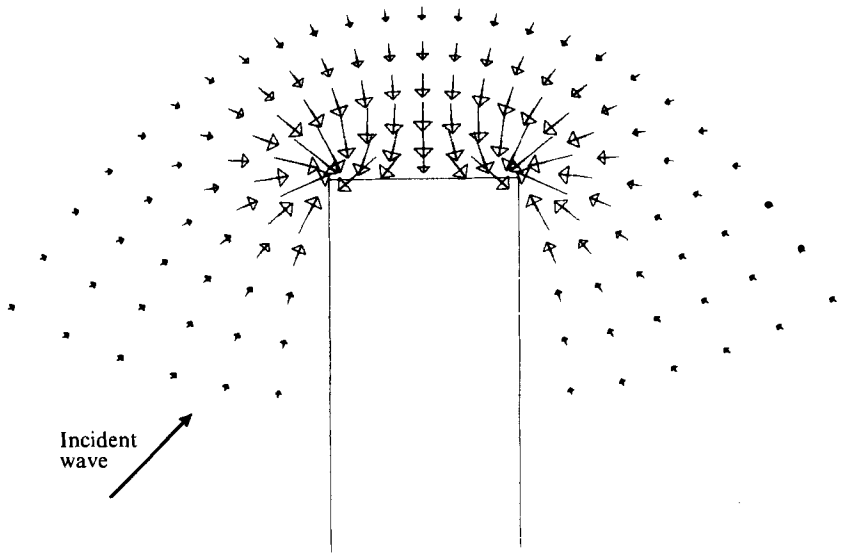

FIGURE 3. Mass transport velocity vectors in gravity waves near the solid bottom in the presence of a breakwater with a rectangular head.

which maps the neighbourhood of the breakwater head from the Z plane to the upper half of the τ plane. The mass transport vector at a height $\xi < 1{\cdot}6$ above the bottom is shown in figure 3. Strong convergence towards the corners is evident. This suggests that mass transport may be partly responsible for the narrowing of a harbour entrance, which then requires dredging to maintain its opening.

Of course, the present prediction fails in the neighbourhood where the local oscillatory current is so large that separation is significant. However, in sufficiently deep water offshore the velocity U_0 can be small enough to avoid separation and yet large enough to move the sediment. The present theory is then relevant, assuming that turbulence in the boundary layer does not alter the qualitative conclusions.

2.3. *Experimental evidence of sediment transport*

A simple demonstration was made at our laboratory with a vertical circular pile of diameter 6·5 cm in a water depth of 16 cm. A standing wave of period 1·125 s and amplitude 2·5 cm was maintained. The depth of the laminar boundary layer below $\xi = 1{\cdot}6$ was $1{\cdot}6\,\delta \cong 1{\cdot}12$ mm. A sediment mixture was then spread sparsely around the cylinder. The mixture consisted of roughly equal portions of beach sand of mean diameter 0·3 mm and Dow Chemical polystyrene spheres of diameter 0·5 mm. The cylinder was placed at a nodal line of the waves where the oscillatory velocity was largest near the bottom. The plastic spheres, being only slightly heavier than water, were easily made to roll on the bottom by the oscillating fluid. On average they first drifted towards the cylinder, but were not deposited there and were bounced away. They served the purpose of mobilizing the much heavier sand, which would otherwise not have been moved by the waves. At first a ring of the floor surrounding the cylinder was wiped clean. Within a few periods sand particles were attracted towards the cylinder and piled up along the diameter parallel to the wave crests. Figure 4 (plate 1)

shows the final view from the side of the wave maker; the dark spots, stripes and patches were covered with sand while the lighter background was the floor covered with a plastic sheet. The sand ripples away from the cylinder were parallel to the wave crests, hence they served to indicate the direction of the latter. The free surface in the neighbourhood was quite rough but the particles beneath oscillated in a predominantly simple harmonic manner as far as the eye could detect.

We also experimented with a long straight estuary of breadth 17·5 cm with a narrow entrance which was formed by attaching two half circular cylinders of diameter 7·5 cm. The entrance was thus smooth and of breadth 10 cm. The free surface in the estuary was somewhat resonated by adjusting the end wall in order to achieve sufficient velocity to move the sand. Deposition was observed near the cylinder at the narrowest points of the entrance, as shown in figure 5 (plate 1). The wave maker was shut off during photography so as to give a clear picture of the bottom. Without rounding the entrance, earlier experiments indicated significant separation near the sharp corners, so that sediment was all swept away.

3. Mass transport in tides near a small body

3.1. *The inviscid flow in the near field*

We shall first recall some results for the inviscid wave field near the body. For simplicity, the ocean depth h is assumed to be constant. To the first order, the free-surface elevation of a simple harmonic tide

$$\zeta_I = \tfrac{1}{2}[\eta e^{i\omega t} + \eta^* e^{-i\omega t}]$$

is again governed by (2.6), with

$$k^2 = \frac{\omega^2}{gh}\left[1 - \left(\frac{2\Omega}{\omega}\right)^2\right], \tag{3.1}$$

where Ω is the angular velocity component along the local vertical, which is

$$2\pi \sin(\text{latitude})/\text{day},$$

also taken to be constant. The velocity field

$$\mathbf{U}_I = \tfrac{1}{2}(\mathbf{U}_0 e^{i\omega t} + \mathbf{U}_0^* e^{-i\omega t})$$

is given by

$$\mathbf{U}_0 = \frac{g}{\omega^2 - \Omega^2}(-i\omega - 2\boldsymbol{\Omega}\times)\nabla\eta. \tag{3.2}$$

On the solid boundary

$$\mathbf{U}_I.\mathbf{n} = \mathbf{U}_0.\mathbf{n} = 0. \tag{3.3}$$

In the neighbourhood of the small body where $ka \ll 1$, (2.1) may again be approximated by Laplace's equation (see, for example, Longuet-Higgins 1970; Buchwald 1971). Buchwald further pointed out that if a complex potential

$$W(Z) = \Phi(x, y) + i\Psi(x, y) \tag{3.4}$$

such that

$$\partial\Phi/\partial n = 0 \quad \text{on the solid body} \tag{3.5}$$

is found then the solution in the near field may be taken as

$$\eta = -\frac{i\omega}{g} C\left(\Phi - \frac{i\Omega}{\omega}\Psi + \text{constant}\right), \tag{3.6}$$

$$\mathbf{U}_0 = C\nabla\Phi, \tag{3.7}$$

where C is an arbitrary complex constant. Thus the near field again reduces to that of a usual potential flow problem for W where some real coefficients as well as C must be determined by matching with the far-field solution. More specifically, when the lateral boundary is a long and straight coastline with a small peninsula or a narrow estuary, the physical domain of Z may be mapped onto the upper half τ plane. For several geometries of practical interest it may be shown that the leading term for W is either τ or $\ln\tau$, i.e.

$$W = \begin{cases} C_0\tau + \text{constant}, & \text{peninsula in a straight coast}, \quad (3.8a) \\ C_1 \ln\tau + \text{constant}, & \text{estuary or bay mouth in a straight coast}, \quad (3.8b) \end{cases}$$

where C_0 and C_1 are real. Combining with (3.7), $\mathbf{U}_0$ is undetermined only up to one complex constant factor CC_0 or CC_1 to the leading approximation. Thus $\mathbf{U}_I$ may be represented by

$$\mathbf{U}_I = \tfrac{1}{2}\mathbf{U}_0[e^{i(\omega t+\gamma)} + e^{-i(\omega t+\gamma)}], \tag{3.9}$$

where $\mathbf{U}_0$ is defined to be real and γ is constant.

It has been pointed out by Moore (1970) that the second-order mean motion in the inviscid region is non-trivial in general. Under the present circumstances, it may be inferred from his conclusions that the mean motion does not interact with the induced stream owing to viscosity and can be treated separately. We give a slightly more direct argument here. The averaged equations for the mean motion $(\langle\mathbf{U}_2\rangle, \langle\zeta_2\rangle)$ at second order are

$$\nabla.\langle h\mathbf{U}_2\rangle + \nabla.\langle\zeta_I\mathbf{U}_I\rangle = 0, \tag{3.10}$$

$$2\boldsymbol{\Omega}\times\langle\mathbf{U}_2\rangle = -g\nabla\langle\zeta_2\rangle - \langle\mathbf{U}_I.\nabla\mathbf{U}_I\rangle. \tag{3.11}$$

By use of the linearized equations of continuity and momentum it can be shown that the second term in (3.10) vanishes. Since h = constant, it follows that $\langle\mathbf{U}_2\rangle$ is solenoidal. Since $\mathbf{U}_I$ is approximately irrotational for small ka, we have

$$\mathbf{U}_I.\nabla\mathbf{U}_I = \tfrac{1}{2}\nabla\mathbf{U}_I^2(1+O[(ka)^2]). \tag{3.12}$$

Upon substituting this result into (3.11) it is easily seen that $\langle\mathbf{U}_2\rangle$ may be 'solved' by

$$\langle\mathbf{U}_2\rangle = \mathbf{u}_g, \quad \langle\zeta_2\rangle = \zeta_g - \langle\mathbf{U}_I^2\rangle/2g, \tag{3.13a,b}$$

where $\langle\mathbf{u}_g, \zeta_g\rangle$ is a geostrophic flow constrained by other global boundary conditions. The term $-\langle\mathbf{U}_I^2\rangle/2g$ in (3.13b) is merely the wave set-down, generating no current in the inviscid region; its gradient, however, plays a dynamic role in the bottom boundary layer as will be evident later. Once $\mathbf{u}_g$ has been found, its effect in the bottom boundary layer is a standard Ekman solution

$$\mathbf{u}_g\{1-\exp[-(1+i)z(\Omega/\nu)^{\frac{1}{2}}]\}$$

and can be added to the wave-induced motion under study; it will therefore be ignored in what follows.

3.2. *The first-order flow in the Stokes boundary layer*

In terms of the small wave slope, the horizontal Eulerian velocity vector is expanded as $\mathbf{u} = \mathbf{u}_1 + \mathbf{u}_2 + \ldots$. The first-order equation is

$$\frac{\partial\mathbf{u}_1}{\partial t} + 2\boldsymbol{\Omega}\times\mathbf{u}_1 - \nu\frac{\partial^2\mathbf{u}_1}{\partial z^2} = \frac{\partial\mathbf{U}_I}{\partial t} + 2\boldsymbol{\Omega}\times\mathbf{U}_I. \tag{3.14}$$

In terms of $\mathbf{u}_1$ the vertical velocity in the boundary layer is obtained from continuity:

$$w_1 = -\delta \int_0^{\xi} \left(\frac{\partial u_1}{\partial x} + \frac{\partial v_1}{\partial y} \right) d\xi, \quad \xi = z/\delta. \tag{3.15}$$

For reference, we remark here that, for a wave period of 12 h and an eddy viscosity of $10 \sim 100\,\mathrm{cm^2/s}$, δ is $3{\cdot}7 \sim 11{\cdot}7$ m. The first-order problem has been solved by Hunt & Johns; their results are summarized below:

$$u_1 = \mathrm{Re}[(U_0 F_1 - V_0 F_2) e^{i\omega t}], \tag{3.16a}$$

$$v_1 = \mathrm{Re}[(U_0 F_2 - V_0 F_1) e^{i\omega t}], \tag{3.16b}$$

where

$$F_1(\xi) = 1 - \tfrac{1}{2}[e^{-(1+i)\alpha\xi} + e^{-(1+i)\beta\xi}], \tag{3.17a}$$

$$F_2(\xi) = \tfrac{1}{2}i[e^{-(1+i)\alpha\xi} - e^{-(1+i)\beta\xi}], \tag{3.17b}$$

with

$$\alpha = (1+f)^{\frac{1}{2}}, \quad \beta = (1-f)^{\frac{1}{2}}, \quad f \equiv 2\Omega/\omega. \tag{3.18}$$

From here on we restrict the analysis to small ka so that U_0 and V_0 again satisfy the Cauchy–Riemann conditions (2.8*b*, *c*). It follows by substituting (3.16) in (3.15) that

$$w_1 = 0. \tag{3.19}$$

In view of (3.9) we take $\mathbf{U}_0$ to be real. For later convenience it is desirable to represent a vector $\mathbf{U} = (U, V)$ in the complex form $\overline{U} = U + iV$ so as to write

$$\overline{U}_I = E\overline{U}_0, \quad \overline{u}_1 = F\overline{U}_0, \tag{3.20a}$$

$$E = \tfrac{1}{2}[e^{i(\omega t+\gamma)} + e^{-i(\omega t+\gamma)}], \tag{3.20b}$$

$$F = \mathrm{Re}(F_1 e^{i\omega t}) + i\,\mathrm{Re}(F_2 e^{i\omega t}), \tag{3.20c}$$

where $F_1(\xi)$ and $F_2(\xi)$ are given by (3.17*a*, *b*).

3.3. *The second-order drift*

At second order the boundary-layer equation is

$$\frac{\partial \mathbf{u}_2}{\partial t} + 2\boldsymbol{\Omega} \times \mathbf{u}_2 - \nu \frac{\partial^2 \mathbf{u}_2}{\partial z^2} = \mathbf{U}_I . \nabla \mathbf{U}_I - \left(\mathbf{u}_1 . \nabla + w_1 \frac{\partial}{\partial z} \right) \mathbf{u}_1. \tag{3.21}$$

For small ka, the right-hand side reduces to

$$\tfrac{1}{2}\nabla(\mathbf{U}_I^2 - \mathbf{u}_1^2) \tag{3.22}$$

on account of (2.8).

It is in the nonlinear terms that the complex representation greatly simplifies the algebra, which would otherwise be prohibitive. We define the complex gradient operator as

$$\overline{\nabla} = \partial/\partial x + i\,\partial/\partial y, \tag{3.23}$$

so that for any $\overline{U} = U + iV$, with U and V real,

$$\overline{\nabla}|\overline{U}|^2 = (\partial/\partial x + i\,\partial/\partial y)(U^2 + V^2) = \overline{\nabla \mathbf{U}^2}. \tag{3.24}$$

Now (3.21) may be written in complex form as

$$\begin{aligned} \partial \overline{u}_2/\partial t + 2i\Omega \overline{u}_2 - \nu\, \partial^2 \overline{u}_2/\partial z^2 &= \tfrac{1}{2}\overline{\nabla}(|\overline{U}_I|^2 - |\overline{u}_1|^2) \\ &= \tfrac{1}{2}(|E|^2 - |F|^2)\overline{\nabla}|\overline{U}_0|^2. \end{aligned} \tag{3.25}$$

The second equality follows from (3.20*a–c*). Upon taking the time average we obtain

$$(\partial^2/\partial\xi^2 - c^2)\langle\bar{u}_2\rangle = -\omega^{-1}\langle|E|^2 - |F|^2\rangle\overline{\nabla}|\bar{U}_0|^2, \tag{3.26}$$

where

$$c = (1+i)f^{\frac{1}{2}}. \tag{3.27}$$

The boundary conditions are

$$\langle\bar{u}_2\rangle = 0 \quad \text{on} \quad \xi = 0, \quad \langle\bar{u}_2\rangle = \text{finite} \quad \text{as} \quad \xi\to\infty. \tag{3.28}$$

The geostrophic flow $\mathbf{u}_g$ is not considered here in view of the remarks at the end of §3.1. The left-hand side of (3.21) can be identified as the differential operator which governs the steady Ekman boundary layer in a rotating fluid. Unlike the classical problem in oceanography, where one encounters a homogeneous Ekman equation with inhomogeneous boundary conditions, the reverse happens here, where the forcing is due to the wave-induced Reynolds stresses throughout the boundary layer. The time average of the right-hand side of (3.26) is easily calculated. Letting

$$\langle\bar{u}_2\rangle = (2\omega)^{-1}H_E(\xi)\overline{\nabla}|\bar{U}_0|^2 \tag{3.29}$$

we obtain

$$(d^2/d\xi^2 - c^2)H_E = -(1 - |F_1|^2 - |F_2|^2), \tag{3.30}$$

where

$$1 - |F_1|^2 - |F_2|^2 = \tfrac{1}{2}(e^{-q\xi} + e^{-q^*\xi} - e^{-2\alpha\xi}) + (e^{-s\xi} + e^{-s^*\xi} - e^{-2\beta\xi})] \tag{3.31}$$

with α and β defined in (2.8) and

$$q = (1+i)\alpha, \quad s = (1+i)\beta. \tag{3.32}$$

The solution satisfying (3.28) may be straightforwardly obtained:

$$H_E = \frac{1}{2}\left[-\left(\frac{1}{q^2-c^2} + \frac{1}{q^{*2}-c^2} - \frac{1}{4\alpha^2-c^2}\right)e^{-c\xi} + \frac{1}{q^2-c^2}e^{-q\xi} + \frac{1}{q^{*2}-c^2}e^{-q^*\xi} - \frac{1}{4\alpha^2-c^2}e^{-2\alpha\xi}\right] - \tfrac{1}{2}[\alpha\to\beta, q\to s], \tag{3.33}$$

where the second bracket consists of the same terms as the first except that α and q must be replaced by β and s, respectively. We point out that, when $f = \frac{1}{2}$, $s = c = (1+i)/2^{\frac{1}{2}}$, and H_E is not singular since $(e^{-s\xi} - e^{-c\xi})/(s^2 - c^2)$ remains finite.

Since most existing analytical results for plane potential flows can be expressed in terms of the complex potential $W(Z)$, it is desirable to rewrite the nonlinear term $\overline{\nabla}|\bar{U}_0|^2$ in (3.26) in terms of W directly. We define W by

$$\bar{U}_0 = U_0 + iV_0 = (dW/dZ)^* = W'^*. \tag{3.34}$$

Note that if $\mathbf{M} = (M_x, M_y)$ is any vector and $\mathbf{N} = (N_x, N_y)$ is any solenoidal and irrotational vector then

$$\mathbf{M}.\nabla\mathbf{N} = \left(M_x\frac{\partial N_x}{\partial x} + M_y\frac{\partial N_y}{\partial x}, \quad M_x\frac{\partial N_y}{\partial y} - M_y\frac{\partial N_x}{\partial x}\right),$$

of which the complex form is

$$\mathbf{M}.\nabla\mathbf{N} = (M_x - iM_y)\frac{\partial}{\partial x}(N_x + iN_y) = \bar{M}^*\frac{d\bar{N}}{dZ}.$$

Accordingly, the complex form of the mean Eulerian drift may be given as

$$\langle\bar{u}_E\rangle \equiv \langle\bar{u}_2\rangle = +\omega^{-1}H_E(\xi)\,W'\,W''^*. \tag{3.35}$$

In order to obtain the Lagrangian mass transport, one must add the Stokes drift

$$\langle \bar{u}_S \rangle \equiv \left\langle \left(\int_{t_0}^{t} \mathbf{u}_1 dt \right) . \nabla \mathbf{u}_i \right\rangle. \tag{3.36}$$

Using (3.16) and (3.17) the right-hand side takes the following complex form:

$$\left\langle F \int_{t_0}^{t} F^* dt \right\rangle \bar{U}_0^* \frac{d\bar{U}_0}{dZ},$$

which can be reduced to

$$\langle \bar{u}_S \rangle = \omega^{-1} H_S(\xi)\, W' W''^*, \tag{3.37}$$

where
$$H_S(\xi) = \tfrac{1}{2}(F_1 F_2^* - F_1^* F_2)$$
$$= -\tfrac{1}{2}i[(e^{-q\xi} + e^{-q^*\xi} - e^{-2\alpha\xi}) - (e^{-s\xi} + e^{-s^*\xi} - e^{-2\beta\xi})], \tag{3.38}$$

after using (3.32). Note that H_S is purely imaginary and vanishes for $f = 0$.

Finally, the total Lagrangian drift is given by

$$\langle \bar{u}_L \rangle = \langle \bar{u}_2 \rangle + \langle \bar{u}_S \rangle = \omega^{-1} H_L W' W''^*,$$

where
$$H_L = H_E + H_S = -\left\{ -\tfrac{1}{2} e^{-c\xi} \left(\frac{1}{q^2 - c^2} + \frac{1}{q^{*2} - c^2} - \frac{1}{4\alpha^2 - c^2} \right) \right.$$
$$\left. + \frac{1}{2}\left[e^{-q\xi} \left(\frac{1}{q^2 - c^2} + \frac{i}{2} \right) + e^{-q^*\xi} \left(\frac{1}{q^{*2} - c^2} + \frac{i}{2} \right) - \left(\frac{1}{4\alpha^2 - c^2} + \frac{i}{2} \right) e^{-2\alpha\xi} \right] \right\}$$
$$+ \{\alpha \to \beta, q \to s, q^* \to s^*\}, \tag{3.39}$$

where the second curly bracket is obtained from the first after the changes indicated.

3.4. *The vertical dependence*

The spatial variation of the horizontal factor $W' W''^*$ is independent of earth rotation, hence it is common to gravity waves and tides. Details depend on the specific geometry of the solid boundaries and will be discussed for a few examples later. The vertical variation of the mass transport through the boundary layer is entirely embodied in the factor $H_L(\xi)$, which depends on $f = 2\Omega/\omega$. For $\Omega = 0$, i.e. gravity waves, we have

$$\alpha = \beta = 1, \quad q = s = 1 + i, \quad c = 0,$$

so H_L reduces to $\frac{1}{4}\operatorname{Re} G_2$, cf. (2.11).

Near the bottom, where heavy sediment is likely to be affected, we approximate $H_L(\xi)$ for small ξ:

$$H_L(\xi) \cong H_L'(0)\xi, \tag{3.40a}$$

where

$$H_L'(0) = +\tfrac{1}{2}\xi \left[\frac{1}{1+i} \left(\frac{1}{f^{\frac{1}{2}} + (1+f)^{\frac{1}{2}}} + \frac{1}{f^{\frac{1}{2}} + (1-f)^{\frac{1}{2}}} \right) + \frac{1}{(1+i)f^{\frac{1}{2}} + (1-i)(1+f)^{\frac{1}{2}}} \right.$$
$$\left. + \frac{1}{(1+i)f^{\frac{1}{2}} + (1-i)(1-f)^{\frac{1}{2}}} - \frac{1}{(1+i)f^{\frac{1}{2}} + 2(1+f)^{\frac{1}{2}}} - \frac{1}{(1+i)f^{\frac{1}{2}} + 2(1-f)^{\frac{1}{2}}} \right] \tag{3.40b}$$

is a complex number and is plotted in figure 6. At the limit $f = 2\Omega/\omega = 0$, $H_L'(0)$ is real. But as f increases, i.e. moving north in the northern hemisphere, there is an

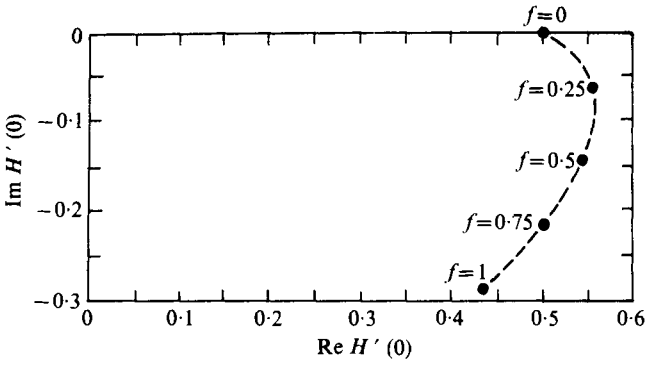

FIGURE 6. The behaviour of $H_L'(0)$ as a function of f.

increasing tendency for H_L to point away from the negative real axis. The neighbourhood of $f = 1$ is excluded from our discussion to avoid singularity in the tidal theory. Let θ_L, θ_1 and θ_2 be the phases of the complex quantities $\langle \mathbf{u}_L \rangle$, $\frac{1}{2}\overline{\nabla}|\overline{U}|^2$ and $H'(0)$. It is clear that $\theta_L = \theta_1 + \theta_2$. Since $\theta_2 < 0$, near the bottom of the boundary layer the mass transport vector $\langle \mathbf{u}_L \rangle$ slants to the right of the vector $\nabla|\mathbf{U}_0|^2$ in the northern hemisphere.

The variation of $H_L(\xi)$ for all ξ is shown in figures 7(*a*), (*b*) and (*c*) for $f = 0{\cdot}25$, $0{\cdot}5$ and $0{\cdot}75$. The general feature is a complicated turning, stretching or shortening of the complex vector H_L as ξ increases. For a larger f the vector wanders away from the real axis to a greater extent. For all $f \neq 0$, $H_L \to 0$ as $\xi \to \infty$, which is the consequence of $w_1 = 0$ owing to the assumption of small ka. Note that, in terms of $\delta = (2\nu/\omega)^{\frac{1}{2}}$, the Stokes-layer thickness, and $\delta_E = (\nu/\Omega)^{\frac{1}{2}}$, the Ekman-layer thickness, the ratio $f = 2\Omega/\omega$ is equal to $(\delta/\delta_E)^2$. Thus in the case $f = 0$ the finite limit shown in figure 1 is occurring at a depth much less than δ_E.

Apart from H_L, the vertical variation of the Eulerian drift H_E may be of interest in ocean circulations; a somewhat related study on large-scale depth-averaged circulation due to periodic wind stresses has been made by Veronis (1966). In figures 8(*a*), (*b*) and (*c*), we show the variation of H_E *vs.* ξ for $f = 0{\cdot}25$, $0{\cdot}5$ and $0{\cdot}75$; the behaviour is different from the Ekman spiral in that $H_E = 0$ for both $\xi = 0$ and $\xi = \infty$. The total horizontal flux within the boundary layer is clearly

$$\mathbf{M}_E = \int_0^\infty \langle \mathbf{u}_2 \rangle d\xi = \frac{\delta}{2\omega} \nabla U_0^2 \int_0^\infty H_E(\xi) d\xi. \tag{3.41}$$

The integral

$$I_E = \int_0^\infty H_E(\xi) d\xi = \frac{1}{2}\left[\frac{1}{qc(q+c)} + \frac{1}{q^*c(q+c)} - \frac{1}{2\alpha c(2\alpha+c)} + \frac{1}{sc(s+c)} + \frac{1}{s^*c(s+c)} - \frac{1}{2\beta c(2\beta+c)}\right] \tag{3.42}$$

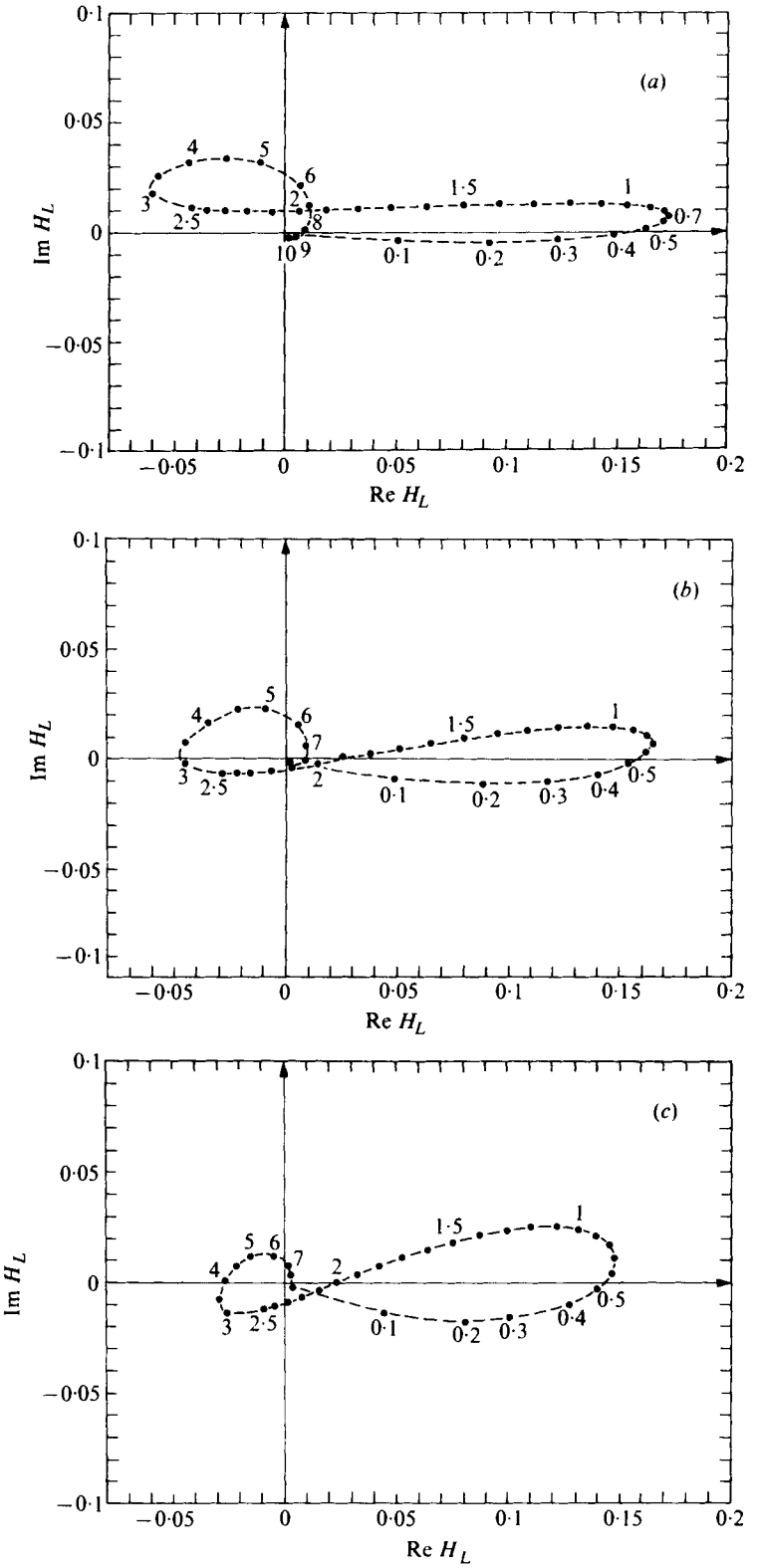

FIGURE 7. The factor H_L representing the vertical variation of the Lagrangian mass transport near a small body owing to long-period oscillations in a rotating fluid. A number near a dot represents the normalized height z/δ above the bottom. The complex vector from the origin to the dot gives the complex factor H_L at that height. (*a*) $f = 0{\cdot}25$. (*b*) $f = 0{\cdot}5$. (*c*) $f = 0{\cdot}75$.

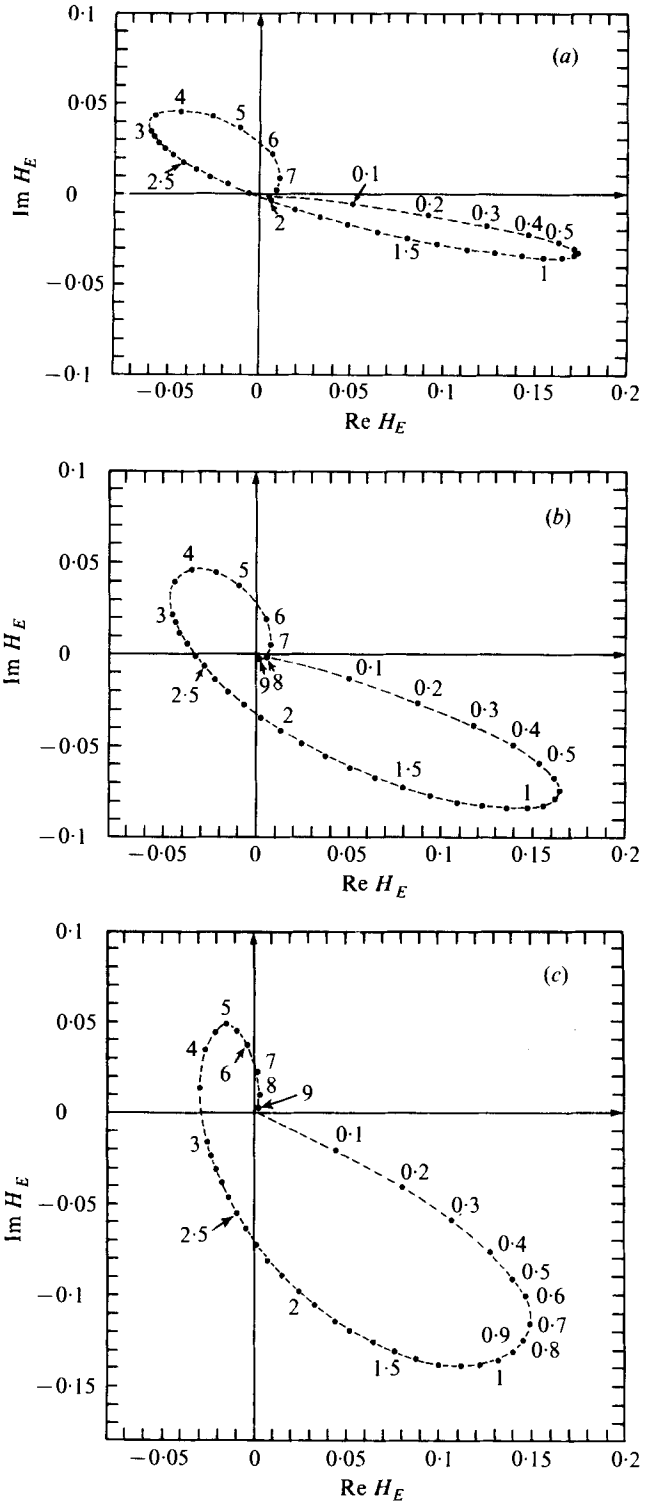

FIGURE 8. The factor H_E representing the vertical variation of the Eulerian induced streaming near a small body owing to long-period oscillations of a rotating fluid. A number near a dot represents the normalized height z/δ above the bottom. The complex vector from the origin to the dot gives the complex factor H_E at that height. (*a*) $f = 0{\cdot}25$. (*b*) $f = 0{\cdot}50$. (*c*) $f = 0{\cdot}75$.

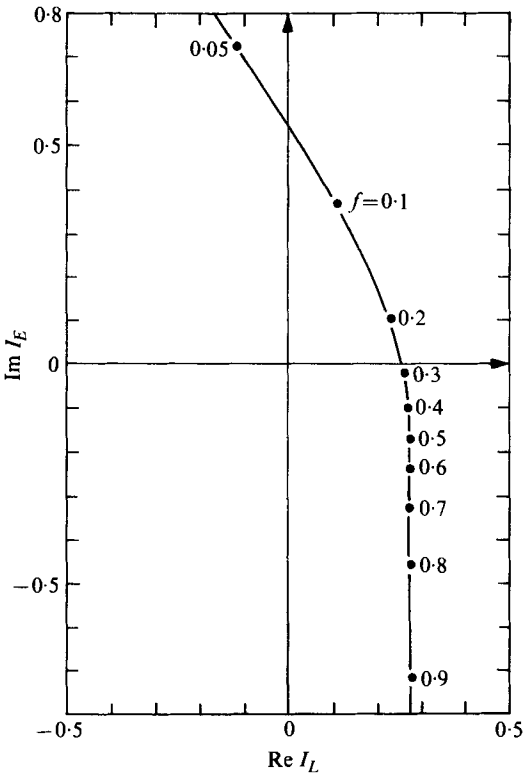

FIGURE 9. The factor I_E for the mean Eulerian flux in the entire bottom boundary layer near a small body owing to oscillations of a rotating fluid. A number near a dot represents the value of $f = 2\Omega/\omega$. The complex vector I_E is obtained by connecting the origin and the dot.

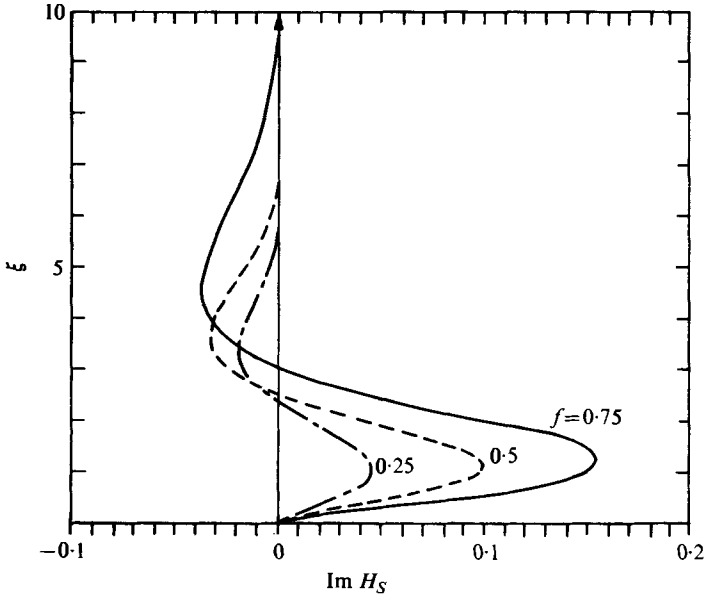

FIGURE 10. The factor $\mathrm{Im}\, H_S$ representing the vertical variation of the horizontal Stokes drift in an oscillatory boundary layer near the bottom of a rotating fluid in the presence of a small body. $\mathrm{Re}\, H_S \equiv 0$.

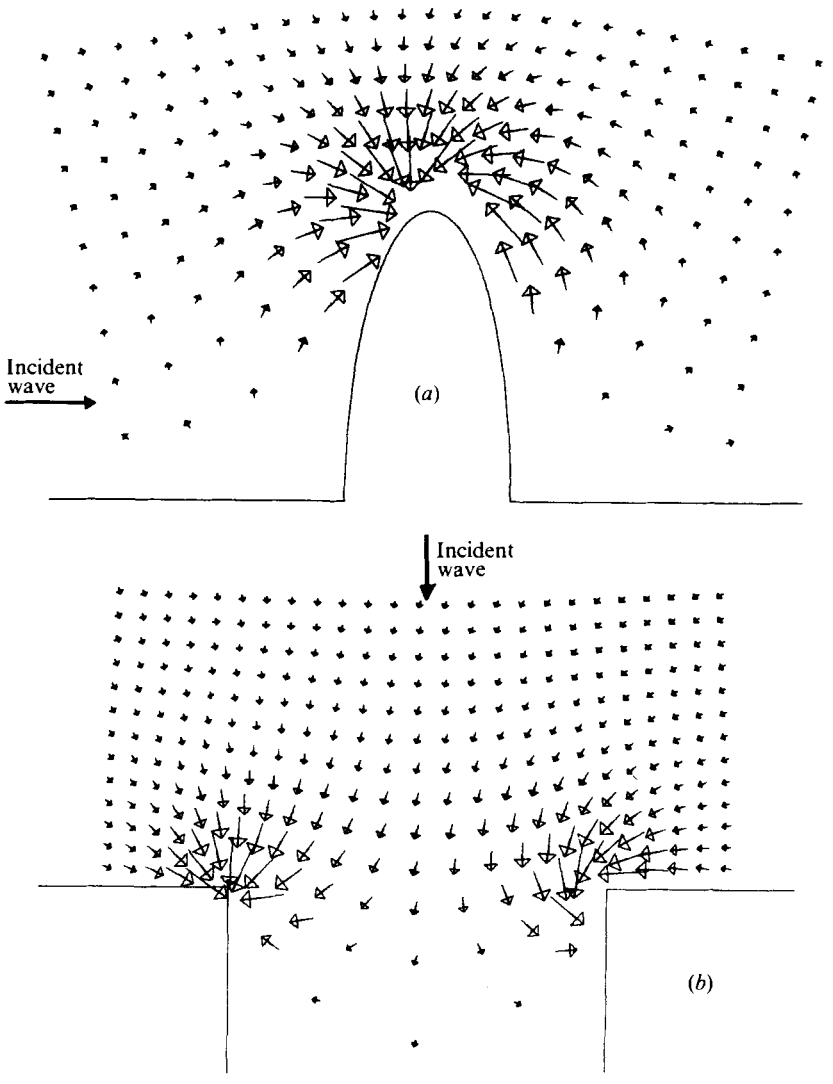

FIGURE 11. Mass transport vectors near the bottom in the presence of (*a*) an elliptical peninsula and (*b*) an estuary. $f = 2\Omega/\omega = 0{\cdot}707$, $\xi = 0{\cdot}1$.

is a continuous function of f and is plotted in figure 9. It is singular at $f = 0$ and 1. This flux, which is caused by the ever-present tides, may be worth attention as a local modification of wind-driven currents.

The quantity H_S, which is purely imaginary, is plotted in figure 10. The corresponding Stokes drift is always at right angles to ∇U_0^2; it is responsible for reducing the directional spread of H_L in comparison to H_E.

3.5. *The horizontal distribution of mass transport*

We plot the horizontal distribution of $\langle \mathbf{u}_L \rangle$ near the bottom $\xi = 0{\cdot}1$ for only an elliptic peninsula (figure 11*a*), and a rectangular estuary (figure 11*b*) in the northern hemisphere. The tide period is assumed to be 12 h and the latitude 45°N, so that

$2\Omega/\omega \cong 0{\cdot}707$. The incident wave in the far field may be a Kelvin wave. All magnitudes are relative.

As pointed out before $\langle \mathbf{u}_L \rangle$ slants to the right of the local vector of $\nabla|\mathbf{U}_0|$. Thus for a peninsula or an estuary along a western (eastern) coast, heavy sediment may tend to accumulate in the neighbourhood slightly to the south (north) of sharp convex corners provided that flow separation is unimportant. The rightward shift increases with latitude. Similar conclusions may be drawn for tidal inlets of rivers or between barrier islands. We stress that, since flow separation is not accounted for here, the sharp corners at an estuary entrance must be rounded for the theory to be relevant. In addition, the definite behaviour of sediment is a complex matter about which our knowledge is meagre. The present deductions from fluid behaviour alone do no more than indicate the tendency.

In closing, we remark that, by removing the assumption of small ka and incorporating the geostrophic flow, an extension of the present analysis on tide-driven mass transport may add to our understanding of the three-dimensional picture of large-scale ocean circulation.

One of the authors (J.L.) thanks the French Administration of Ponts et Chaussées for making possible his stay at M.I.T. Partial support of this work has been received from the Fluid Dynamics Program, U.S. Office of Naval Research. It is also our pleasure to thank Mr D. K. P. Yue and Mr David Smith for their assistance, and Dr Philip L. F. Liu for participation at the initial stage of this research. Thanks are also due to a referee for bringing our attention to the paper by Moore.

REFERENCES

Buchwald, V. T. 1971 The diffraction of tides by a narrow channel. *J. Fluid Mech.* **46**, 501–511.

Carter, T. G., Liu, P. L-F. & Mei, C. C. 1973 Mass transport by waves and offshore sand bedforms. *J. Waterways, Harbors Coastal Engng, Div. A.S.C.E.* **99**, 165–184.

Crighton, D. G. & Leppington, F. G. 1973 Singular perturbation methods in acoustics: diffraction by a plate of finite thickness. *Proc. Roy. Soc.* A **335**, 313–339.

Horikawa, K. & Watanabe, A. 1968 Laboratory study on oscillatory boundary layer flow. *Proc. 12th Conf. Coastal Engng*, vol. 1, pp. 467–486.

Hunt, J. N. & Johns, B. 1963 Currents induced by tides and gravity waves. *Tellus* **15**, 4.

Johnson, I. G. & Carlsen, N. A. 1976 Experimental and theoretical investigations in an oscillatory turbulent boundary layer. *J. Hydraul. Res.* **14**, 45–60.

Lamoure, J. 1976 Effects of topographical variations on mass transport in oscillatory flows. M.S. thesis, Dept. Civil Engineering, Massachusetts Institute of Technology.

Lau, J. & Travis, B. 1973 Slowly varying Stokes waves and submarine longshore bars. *J. Geophys. Res.* **78**, 4489–4498.

Longuet-Higgins, M. S. 1953 Mass transport in water waves. *Phil. Trans. Roy. Soc.* A **245**, 535–581.

Longuet-Higgins, M. S. 1970 Steady currents induced by oscillations round islands. *J. Fluid Mech.* **42**, 701–720.

Mei, C. C. & Ünlüata, Ü. 1976 Resonant scattering by a harbor with two coupled basins. *J. Engng Math.* **10**, 333–353.

Moore, D. 1970 The mass transport velocity induced by force oscillations of a single frequency. *Geophys. Fluid Dyn.* **1**, 237–247.

Rayleigh, Lord 1883 On the circulation of air observed in Kundt's tubes, and some allied acoustical problems. *Phil. Trans. Roy. Soc.* **175**, 1–21.

Veronis, G. 1966 Generation of mean ocean circulation by fluctuating winds. *Tellus* **18**, 66–76.

FIGURE 4. Wave-induced sand accumulation near a circular cylinder. Dark spots, stripes and patches indicate sand. The wave crests are parallel to the ripple crests. Sand particles were removed initially from a ring of width 3 cm surrounding the cylinder.

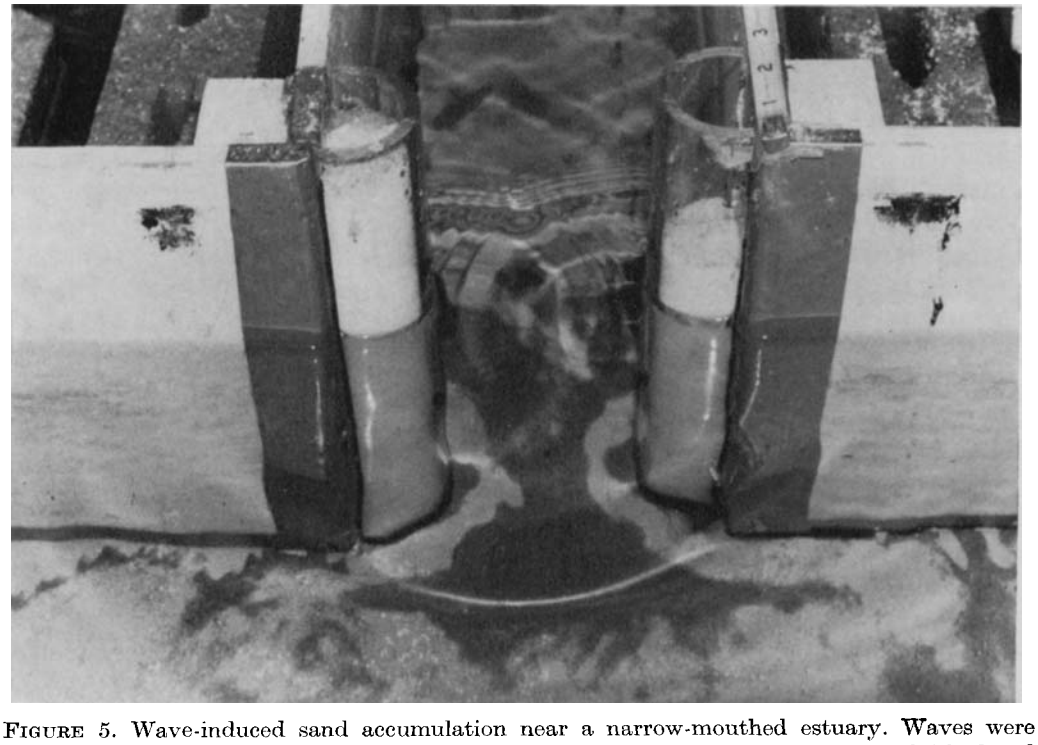

FIGURE 5. Wave-induced sand accumulation near a narrow-mouthed estuary. Waves were normally incident. The wave maker was shut off after the accumulation was established and before photography.